LAWRENCE
LIVERMORE
NATIONAL
LABORATORY

LLNL-JRNL-410877

Multireference - Møller-Plesset Perturbation Theory Results on Levels and Transition Rates in Al-like Ions of Iron Group Elements

J. A. Santana, Y. Ishikawa, E. Träbert

February 26, 2009

Physica Scripta

Disclaimer

Multireference - Møller-Plesset perturbation theory results on levels and transition rates in Al-like ions of iron group elements

Juan A Santana[1], Yasuyuki Ishikawa[1], and Elmar Träbert[2,3]

1 Department of Chemistry and the Chemical Physics Program, University of Puerto Rico, P. O. Box 23346, San Juan, Puerto Rico 00931-3346, USA
2 Astronomisches Institut, Ruhr-Universität Bochum, D-44780 Bochum, Germany
3 Physics Division, LLNL, P.O. Box 808, Livermore, CA 94551, USA

E-mail: traebert@astro.rub.de

Abstract.

Ground configuration and low-lying levels of Al-like ions contribute to a variety of laboratory and solar spectra, but the available information in data bases is neither complete nor necessarily correct. We have performed Multireference - Møller-Plesset perturbation theory calculations that approach spectroscopic accuracy in order to check on the information that data bases hold on the 40 lowest levels of Al-like ions of iron group elements (K through Ge), and to provide input for the interpretation of concurrent experiments. Our results indicate problems of the data base holdings on the levels of the lowest quartet levels in the lighter elements of the range studied. The results of our calculations of the decay rates of five long-lived levels ($3s^2 3p\ ^2\mathrm{P}^\mathrm{o}_{3/2}$, $3s3p^2\ ^4\mathrm{P}^\mathrm{o}_J$, $3s3p3d\ ^4\mathrm{F}^\mathrm{o}_{9/2}$) are compared to lifetime data from beam-foil, electron beam ion trap and heavy-ion storage ring experiments.

PACS numbers: 3270Cs, 3115am, 3450Fa

Submitted to: *Phys. Scr.*

1. Introduction

Ions with a single electron outside of closed shells have been of high interest for spectroscopy because of their prominent resonance lines and for theory because of their perceived simplicity. Detail studies over the decades have revealed how complex the role of the inner electronic shells and their virtual excitations can be. Nevertheless, high accuracy has been achieved in both spectroscopy (Li-, Na- and Cu-like ions up to uranium (Z=92)) and many-body perturbation theory calculations [1, 2]. A second electron in the valence shell introduces massive complications; while experiment can reach the same accuracy as for one-electron spectra, theory has been struggling. Calculations of Al-like ions sometimes have been extensive, but have covered only

a single element at a time [3, 4, 5, 6, 7, 8, 9, 10, 11, 12, 13, 14], or employed rather few configurations when tabulating results for a full isoelectronic sequence [15, 16, 17, 18, 19, 20, 21]. (These citations to theoretical work as well as the ones to experimental data below represent typical samples, but are certainly incomplete; for example, Wei *et al* [22] have calculated n=3-4 transitions in various ions, but these transitions play no role in the present discussion.) Beyond the lowest charge state ions of the Al sequence, the experimental data base has been growing in bursts, whenever specific techniques or devices (beam foil spectroscopy, laser-produced plasmas, tokamaks) gave access to a new range of charge states or observation options [23, 24, 25, 26, 27, 28, 29, 30, 31, 32, 33, 34, 35, 36, 38, 37, 39, 40, 41, 42, 43, 44]. Several attempts have been made to compare calculated results and measurements, with the aim of establishing isoelectronic trends that would be useful for interpolation or extrapolation to ion species not directly covered, often introducing semiempirical corrections to the calculations [45, 46]. These attempts usually were limited to a sample of levels, for example to the $3s3p^2$ quartet term and its intercombination decays, or the $3s3p3d$ $^4\mathrm{F}^\mathrm{o}_J$ levels some of which are exceptionally long-lived [7, 47, 48].

The quality of the experimental data hinges on the observation conditions. While the resonance lines are easily excited, the population of long-lived levels often depends on the particle density in the light source; very-long lived levels may be quenched by collisions. In beam-foil spectroscopy, the emission from long-lived levels is spread out so much that per unit length of ion beam observed the signal rate may be extremely low, and ultimately too low to be significant. In that case, a low-density plasma such as is available in an electron beam ion trap may be the laboratory light source of choice for measurements of electric-dipole (E1) forbidden transitions. Near the low end of the isoelectronic sequence, levels which have spin-changing transition decay channels only (the intercombination decays of the $3s3p^2$ $^4\mathrm{P}_J$ levels) also have very long lifetimes. Consequently, for many elements in that range the positions of the quartet levels have not been established from direct observations of their decays to the ground state, but indirectly via chains of other transitions. Therefore inconsistencies of the tabulated level energies are to be expected more in this range than in others.

Only very recently our multireference - Møller-Plesset (MR-MP) perturbation theory approach has reached an accuracy comparable to that of recent measurements of Zn-like ions at electron beam ion traps [49]. A third electron in the valence shell is expected to cause even more problems for calculations, especially if the first two electrons are no more locked in a ns^2 configuration, but possibly excited. However, recent calculations by our technique of the fine structure splitting and M1 transition rate of the $3s^23p$ $^2\mathrm{P}^\mathrm{o}$ ground term of Al-like Fe (Z=26) have reproduced the spectroscopically known interval and the transition rate [50] without any need for a 'semiempirical' correction. From this success we take the encouragement to extend the calculations to all levels up to the $3s3p3d$ configuration of Al-like ions of iron group elements from potassium (K, Z=19) to germanium (Ge, Z=32). The resonance and intercombination lines of these elements have partly been seen in a variety of light sources, from laser-produced plasmas, foil-

excited ion beams, and ion clouds in electron beam ion traps to the solar corona. Because of the different particle densities in such light sources, the level populations differ drastically, and line intensities may be exploited for plasma diagnostics. The diagnostics usually involves radiative-collisional modeling, which depends rather crucially on the level lifetimes of the more long-lived levels (with radiative decay rates of the same order of magnitude as the collision rates). For this reason, we also present lifetime results for five long-lived levels among the lowest 40 levels, and compare our results to the energy level holdings of data bases [39, 51] and to the results of lifetime measurements.

2. Computational details

Levels and level lifetimes of Al-like ions have been computed by a variety of techniques before, employing nonrelativistic and relativistic techniques (see, for example, [15, 16, 17, 19, 20, 21]). Among those studies, Huang [17] has covered the elements up to Z=92, but used a rather small number of configurations in multiconfiguration Dirac-Fock (MCDF) calculations. The observation along the isoelectronic sequence of line intensity anomalies due to level mixing underlines the need for detail in the description of Al-like ions [52]. Gupta and Msezane have treated a selection of elements using the CIV3 code with a large number of configurations [4, 5, 6, 7, 8, 9, 10, 11, 14]. Compared to all such earlier work, we expect higher accuracy than has been available before, and that from *ab initio* calculations, in contrast to earlier calculations (like those by Fawcett [16] who used a version of the Hartree XR Cowan code [53]) that involved the scaling of parameters to match the experimental level structure. Such scaled calculations are very helpful for interpolating (and slightly extrapolating) experimental data. However, in order to judge the quality and consistency of experimental data sets, *ab initio* calculations should be particularly useful, because the results are not biased by human interference.

Theoretical background information and computational details of the combined state-averaged Multi-Configuration Dirack-Fock (MCDF) Self Consistent Field (SCF) plus state-specific Multi-Reference Møller-Plesset (MR-MP) method, as well as a number of theoretical transition probabilities have been presented elsewhere [49, 50, 54, 55, 56, 57, 58, 59, 60]. Essentially, the method consists of three basic steps. The process begins with a state-average MCDF-Breit (MCDFB) SCF calculation for the ground and low-lying excited states of the ion, to obtain a common set of core and valence spinors in the V^N potential. This is followed by a relativistic multireference Configuration Interaction (CI) procedure [61], including the calculation of highly excited states, in order to account for near-degeneracy effects or strong configuration mixing among the excited states. The relativistic CI, however, fails to account for the bulk of dynamic correlation among all levels unless a very larger number of configuration, on the order of 1×10^6, are included in the CI calculations. The residual dynamic correlation corrections, however, can easily be accounted for by state-specific MR-MP calculations based on the CI wave functions. In this section we briefly outline the computational details to calculate the energy terms and transition probabilities for the aluminium isoelectronic sequence from K^{+6} to Ge^{+19}.

The large and small radial components of the bound Dirac spinors were expanded in sets of even-tempered Gaussian-type functions (GTF) that satisfy the boundary conditions associated with the finite nucleus [62] and are automatically kinetically balanced [63]. The speed of light is taken to be 137.0359895 a.u. throughout this study. For all the systems investigated, even-tempered basis sets of $26s24p22d20f18g18h$ Gaussian spinors for up to angular momentum $L = 5$ and 15 Gaussian spinors for $L = 6 - 11$ are employed. The order of the partial-wave expansion L_{max}, the highest angular momentum of the spinors included in the virtual space, is L_{max}=11 throughout this study. The nuclei were simulated as spheres of uniform proton charge with the radii (Bohr) $R = 2.2677 \times 10^{-5} A^{1/3}$, where A(amu) is the atomic mass number.

The state-average MCDFB SCF calculations for the ground and low-lying excited $J = 1/2 - 5/2$ states in Al-like ions were carried out including seven even- and odd-parity Configuration State Functions (CSFs) arising from the $3s^2 3p^1$, $3s^1 3p^2$, $3p^3$ and $3s^2 3d^1$ configurations. Subsequent relativistic CI includes all the CFSs arising from the configurations, $3s^m 3p^n 3d^p$ with $m + n + p = 3$ (complete active space of the $n = 3$ manifold) to ensure that the $n = 3$ eigenstates of the matrix CI equation are the upper bounds to the exact Dirac-Coulomb-Breit (DCB) energies. A total of 145 CSFs of $J = 1/2 - 9/2$, 72 even-parity, and 73 odd-parity CSFs, thus produced, were included in the CI calculations. Subsequently, each of the 145 eigenstates was subjected to state-specific MR-MP refinement to account for the residual dynamic correlation. All electrons have been included in the MR-MP perturbation theory calculation to determine accurately the effects of relativity on electron correlation. Radiative corrections, the Lamb shifts, were estimated for each state by evaluating the electron self-energy and vacuum polarization following an approximation scheme discussed be Indelicato, Gorceix, and Desclaux [64].

MR-MP calculations of electric multipole transition probabilities in the Babushkin and Coulomb gauge have been discussed in more detail in an earlier study [50]. Because of the strong coupling between the large and small components of the Dirac 4-spinors in the electric multipole transition matrix elements, the transition probability evaluated by excluding the negative-energy space in the Coulomb gauge is inaccuarate and deviates from the value evaluated in the Babushkin gauge. When contributions from the negative-energy space are included, transition probabilities evaluated in the Coulomb gauge approach those evaluated in the Babushkin gauge. In the present study, electric dipole transition probabilities were evaluated in the Babushkin and Coulomb gauges including negative-energies following the method given in [50].

3. Levels

The results of our calculations of the lowest 40 energy levels of Al-like ions of K through Ge are listed in tables 1, 2, 3, 4, 5, 6, 7, 8, 9, 10, 11, 12, 13, 14. Because Fe XIV is of particular interest in astrophysics, we have placed the level identifications with the Fe data in table 8. The level numbers in the other tables can thus be identified by

reference to the first table. We compare our level values with the data found in the NIST on-line data base [51], because this reflects the experimental knowledge and the varying degree of completeness of information on Al-like ions of various elements. For K, Ca, Sc, Cu, Zn, and Ga the NIST data base holdings are rather slim, for Ti through Ni the data collection is almost complete (for the first 40 levels in Al-like ions), and for Ge it is somewhere in the middle. The difference between the NIST listed values and our calculational results is typically much below 0.05% (often better than 0.02%) for the levels in the more completely known spectra. The deviations are clearly larger for many (not all) of the levels in the incompletely known spectra. This scatter suggests that the 'known' data are not just incomplete, but also of lesser quality. Examples are the $3s3p^2$ quartet levels in K, Ca, Sc (with a 1% deviation), the $3s3p3d$ quartet levels in K, Ca, Cu, and Ge (and no data for Zn and Ga), and the $3p^3\ ^4S_{3/2}$ level in Ca and Sc. Seeing the excellent agreement of experimental and calculated energy levels in the elements from Ti through Ni, it appears as a straightforward suggestion that where experimental data are missing, our results can serve as a valid guide. The systematics moreover indicate the aforementioned cases of doubt about the accuracy of some of the listed experimental level data; using our calculational results instead should be a safe bet.

4. Lifetimes

In the Al-like ions of the iron group elements, five excited levels are much longer lived (by roughly two to eight orders of magnitude) than the others. These levels are the upper fine structure level of the ground term, $3s^23p\ ^2P^o_{3/2}$ (decaying by M1 and a very weak E2 transition), the three lowest quartet levels, $3s3p^2\ ^4P_{1/2,3/2,5/2}$ (decaying by spin-changing E1 transitions), and the $3s3p3d\ ^4F^o_{9/2}$ level (with E1-forbidden decay channels only). We discuss the levels in this sequence, before showing how they are connected in plasma diagnostics and in some lifetime measurements. For an example (Fe XIV) of our results on transition rates and level lifetimes, see table 15.

4.1. $3s^23p\ ^2P^o_{3/2}$ *level*

The magnetic dipole (M1) transitions between the fine structure levels of the ground configuration of B-, F-, Al- and Cl-like ions figure prominently in the observations and interpretation of solar and stellar coronae and of low-density laboratory plasmas. They represent radiative decay after excitation to the lowest excited levels of these ions and thus serve as tracers that indicate the presence of a given element and charge state and therefore help to estimate the plasma temperature. However, in a low-density plasma the collision rate for such excitation is often compatible to the M1 radiative decay rate; hence the upper level population depends on the collision rate and thus on density. Depending on the population balance of the lowest levels, certain line intensity ratios in the spectra can then be used as a plasma diagnostic tool that reveals the density. Since

there are many pathways to excitation and deexcitation, collisional-radiative models are employed to take into account hundreds or thousands of levels and tens of thousands of transitions. Very few experimental data exist or will ever become available for the transition rates especially between high-lying levels. Most transitions between low- and high-lying levels can be approximated by using hydrogenic wave functions. In practice, of ions of iron group elements, only some in-shell transition rates have been measured by beam-foil spectroscopy, and some of the E1-forbidden transition rates have been determined experimentally by employing either a heavy-ion storage ring or an electron beam ion trap. It is exactly the latter transition rates that matter most as a testable parameter in the collisional-radiative models. Consequently, these M1 rates (the small E2 admixture amounts to less than 0.1% in the Al-like ions of interest) have been calculated frequently (see [65]), but with varying success (see figure 1).

At a first glance, most of the results (for the example of Fe XIV) fall into a very narrow interval, while very few deviate drastically from that majority. A closer inspection, however, reveals that most of the theoretical results are actually not the results of extensive calculations, but of so-called semiempirical adjustments' to the extensively calculated values. This seemed appropriate, because in a straightforward approximation (near the nonrelativistic limit and assuming rather pure configurations), the M1 transition rate between fine structure levels of a given term is the product of the line strength S and the third power of the transition energy ΔE. For the transition of interest in the ground term of Al-like ions, Racah algebra in this approximation yields $S = 4/3$, and the transition energy is available with high accuracy from spectroscopic observations. If a calculation does not determine the transition energy correctly, it is quite customary to replace the faulty energy difference by the experimental data - the aforementioned 'semiempirical' correction. Most calculations did not achieve good agreement with the experimental transition energy (the fine structure interval), but after the correction one does not see that shortfall of an extensive calculational effort. So the few deviant theory results displayed in figure 1 are those that were not corrected and thus give a more honest presentation of the shortcomings of earlier calculations. There also are early *ab initio* calculations that - although working with rather few wave functions - come close to the expected result, but only in this particular case (and not in others); here the agreement has to be considered as merely incidental.

We note that our own computational technique has determined the ground state fine structure interval in Fe XIV very close to the experimental value, so that no semiemprical correction was necessary [50]. The calculated $3s^2 3p\ ^2\mathrm{P}^{\mathrm{o}}_{3/2}$ level lifetime agrees with the result of a measurement at the Livermore electron beam ion trap (EBIT) [66]. The calculation did not comprise a QED correction to the M1 transition operator that has since been discussed [67, 68]. This QED correction increases the transition rate by a factor $(1 + 2\alpha/\pi)$, or by 0.45%. After this correction, the MR-MP result slightly disagrees with the Livermore result. (Agreement within one standard deviation of the experimental result would be restored, if the experiment suffered from a systematic error discussed below and was corrected accordingly.) The Heidelberg EBIT group

has measured the same atomic system and has claimed an error bar of only 0.1%. At this level of precision, the experimental finding disagrees with all calculations. We will discuss this problem in the context of experiments below. In table 16 we list our calculated level lifetimes for the range of Al-like ions from K through Ge.

4.2. $3s3p^2\ {}^4P_J$ *levels*

The (spin-changing) intercombination decay rate of the lowest quartet levels is much higher than the M1 transition rate discussed above. The order of magnitude of the level lifetimes (for Fe XIV) is 100 ns versus 17 ms. The many-nanosecond lifetime range is accessible by beam-foil spectroscopy, and the intercombination transitions in Al-like ions of Fe, Co, Ni, Cu, and Zn (see [23, 24] and later papers by the same authors) were detected by beam-foil spectroscopy at Bochum at around the same time as Sugar *et al.* reported the lines for ions of Cu through Mo from a tokamak [25]. The beam-foil observations were not very accurate, but they made it possible to recognize the same lines in EUV spectra of the solar corona, where the wavelengths had been measured with much better accuracy, but where the lines had remained unidentified. The Bochum beam-foil work was extended to Br at Argonne [40] and to Au at GSI Darmstadt [43, 44], including some lifetime determinations. A group from Lund pursued similar work at RIKEN (Japan), but their lifetime results follow a different isoelectronic trend that disagrees with theory [41, 42]. At the low-Z end of the isoelectronic sequence, Si^+ has been studied in a radiofrequency ion trap [69]. For moderate charge states, the isoelectronic trends of the fine structure intervals of the quartet levels have been systematized on the basis of the experimental data [24, 45]. Such data of sufficient quality are not yet available for most low-charge state ions of the Al isoelectronic sequence, because in most plasmas the emission of the ions in long-lived low quartet levels would be quenched by collisions.

4.3. $3s3p3d\ {}^4F^o_{9/2}$ *level*

The $3s3p3d\ {}^4\mathrm{F}^o_{9/2}$ level might seem to be of little interest, because it has a J value so high that there is no E1 excitation from the ground term, and the $3s3p3d$ configuration is multiply excited. It is probably for these reasons that various calculations of energy levels have left out this level altogether, even when explicitly treating the other levels of the same quartet term. The level values of some of the $3s3p3d\ {}^4\mathrm{F}^o_J$ levels in Al-like ions of iron group elements have first be determined by Churilov and Levashov [48] who obtained these data as the lower levels of decays that started out from $3p^23d$ and $3s3d^2$ levels in a laser-produced plasma. Practically coincidentally, but employing a very different technique, several of the levels were seen in emission after foil excitation of fast ion beams [47]. The latter experiment exploited the relative longevity of the high angular momentum quartet levels ($J = 3/2$ to $7/2$) with their lifetimes in the nanosecond range (whereas most other levels and thus spectral lines featured picosecond lifetimes). Waiting out the decay of the short-lived levels, the delayed spectrum is expected to

be relatively enriched in contributions from long-lived elevels, but, of course, over time all of the decay curves are being reduced in intensity. Owing to a low signal rate, the spectral resolution had to be no better than moderate, and some spectral blends were unavoidable. Hence, while the lifetime pattern reported is qualitatively compatible with various calculations, the experimental lifetime data are not good enough for a meaningful comparison with theory in quantitative detail. The beam-foil technique was not suitable to deal with the much longer lifetime of the $3s3p3d\ ^4\mathrm{F}^\mathrm{o}_{9/2}$ level for which calculations apparently did not even exist at the time. Later calculations pointed to the millisecond range, that is, to a lifetime six orders of magnitude longer than those of the three other fine structure levels of the same term. (A similarly wide range of fine structure level lifetimes is found for the $3s^23p3d\ ^3\mathrm{F}^\mathrm{o}$ term in Si-like ions, where $J = 4$ is the long-lived fine structure level [70, 71].) The calculated lifetimes of the $3s3p3d\ ^4\mathrm{F}^\mathrm{o}_{9/2}$ level in the ions of present interest are included in table 16.

4.4. Cascade problem in measurements

The lifetimes of the $3s^23p\ ^2P^\mathrm{o}_{3/2}$ level and the $3s3p3d\ ^4\mathrm{F}^\mathrm{o}_{9/2}$ level turn out to be rather similar to each other. This may be seen as a curiosity of little consequence. However, in a recent lifetime measurement at a heavy-ion storage ring, the similarity has caused a sizeable systematic error [70]. On its own, this finding would also be of rather limited interest, but it might pertain - to a much smaller extent, but of a relatively high importance - to the extremely precise lifetime measurements performed at the Heidelberg electron beam ion trap [67, 68]. The details of the causal chain are yet to be determined, but preliminary radiative-collisional modeling estimates indicate that the cascade from the $3s3p3d\ ^4\mathrm{F}^\mathrm{o}_{9/2}$ level might cause a shift of the apparent $3s^23p\ ^2P^\mathrm{o}_{3/2}$ level lifetime by a small fraction of one percent, and thus by clearly more than the present error estimate of that experiment - an experiment the lifetime result of which disagrees with modern quantum mechanical calculations that take all known QED contributions (to the energy and to the M1 transition operator) into account. In Fe XIV, our MR-MP calculations indicate three major decay branches of the $3s3p3d\ ^4\mathrm{F}^\mathrm{o}_{9/2}$ level: an M1 transition with a branch fraction of 29.3% leads to the $3s3p3d\ ^4\mathrm{F}^\mathrm{o}_{7/2}$ level from which in turn E1 transitions feed the $3s^23d\ ^2\mathrm{D}$ and $3s3p^2\ ^2\mathrm{D}$ and $^4\mathrm{P}\ J = 5/2$ levels, all of which feed into $3s^23p\ ^2\mathrm{P}^\mathrm{o}_{3/2}$. From the same original level, M2 transitions with branch fractions of 64.3% and 6.4%, respectively, lead directly to the same $3s^23d\ ^2\mathrm{D}$, $3s3p^2\ ^2\mathrm{D}$ and $3s3p^2\ ^4\mathrm{P}\ J = 5/2$ levels. Practically the complete population of the $3s3p3d\ ^4\mathrm{F}^\mathrm{o}_{9/2}$ level thus feeds the $3s^23p\ ^2\mathrm{P}^\mathrm{o}_{3/2}$ level, the upper one of the fine structure levels of the ground term. When recording and analyzing decay curves of the $^2\mathrm{P}^\mathrm{o}_{3/2}$ level in Fe XIV, the lifetimes of the primary decay and the specific cascade cannot be separated by multi-exponential analysis. However, because of the Z^4 scaling of fine structure splittings, the M1 decay rate in the $3s3p3d\ ^4\mathrm{F}^\mathrm{o}$ term grows faster with nuclear charge Z than the M2 decay rates, giving the M1 decay a branch fraction of almost 50% in Ni XVI, while the overall cascade picture remains the same. The lifetime difference, nevertheless, becomes large

enough to actually see the two different lifetime components in the decay curve, with fit results that corroborate the present calculations [70].

5. Discussion and conclusions

The present study demonstrates how a large body of experimental data on atomic levels can be checked for consistency against the results of *ab initio* calculations that reach close to spectroscopic accuracy without parametrizations or semiempirical adjustments. In this way it becomes apparent where experimental problems remain to be overcome. The question arises, of course, whether it would be cost effective to close the gaps in the data base by further experiments or - given the present high level of accuracy of our calculations - by computation, once the quality of the method has been ascertained. Certainly calculations need to be checked against good experimental data, and, similarly certainly, dedicated experiments may be more accurate than any approximative theoretical description.

Concerning transition probabilities, experiment has been struggling to achieve error bars of less than a few percent, even in favorable cases. However, theory for a long time has not tended to indicate even estimates of uncertainty, and eventually mismatches between experiment and theory have been found that - depending on the atomic system and transition type - ranged from zero to factors of five or more. In the atomic system of present interest, we have concentrated on the five long-lived levels in the $n = 3$ shell. Measurements of the M1 transition rate in the ground term have reached an accuracy of well below 1%, a level at which the QED correction to the M1 transition operator plays a role. Without the EAMM correction to the M1 transition operator, our calculation is in agreement with the outcome of an experiment that carries an 0.7% error bar. If the estimate of a systematic error due to the $3s3p3d$ cascade even under the low-density conditions of an electron beam ion trap is applied to the former data, the agreement holds also for the QED-corrected lifetime. No present calculation agrees with the result of a largely similar experiment that has been stated to carry a 0.1% error. For the lowest quartet levels and their spin-changing E1 decay, the agreement between theory and experiment (which is not very precise in this case) is reasonable; we note that measurements exist only for the $J = 1/2$ and $5/2$ levels, whereas the longer-lived $J = 3/2$ level remains unmeasured. For the $3s3p3d$ $J = 9/2$ level, we present the first calculations for a series of elements. Cascade repopulation from this level has been invoked to explain a systematic shift of lifetime results at a heavy-ion storage ring from the results obtained at electron beam ion traps. In a single case, experiment has derived information on the cascade (in Al-like Ni), and the result is close to our prediction. In these measurements of long atomic lifetimes, experiment apparently will need further refinement before the actual level of validity of our calculations can be tested.

Acknowledgments

ET acknowledges travel support from the German Research Association (DFG). Part of this work has been performed at LLNL under the auspices of the USDoE under contract No. DE-AC52-07NA27344. YI acknowledges partial support from LLNL subcontracts No. B568401 and B579693. Work at the UPR was supported by the Fondo Institucional para la Investigacion (FIPI).

References

[1] Kim Y-K, Baik D H, Indelicato P and Desclaux J P 1991 *Phys. Rev.* A **44** 148
[2] Blundell S A 1993 *Phys. Rev.* A **47** 1790
[3] Froese Fischer C and Liu B 1986 *At. Data Nucl. Data Tables* **34** 261
[4] Gupta G P and Msezane A Z 2002 *Phys. Scr.* **66** 354
[5] Gupta G P and Msezane A Z 1999 *J. Phys. B: At. Mol. Opt. Phys.* **32** 3361
[6] Gupta G P and Msezane A Z 2004 *Phys. Scr.* **69** 273
[7] Gupta G P and Msezane A Z 2004 *Phys. Scr.* **70** 235
[8] Gupta G P and Msezane A Z 2007 *Phys. Scr.* **76** 225
[9] Gupta G P and Msezane A Z 2001 *J. Phys. B: At. Mol. Opt. Phys.* **34** 4217
[10] Gupta G P and Msezane A Z 2005 *At. Data Nucl. Data Tables* **89** 1
[11] Gupta G P and Msezane A Z 2008 *Eur. Phys. J.* D **49** 157
[12] Bhatia A K and Doschek G A 1999 *At. Data Nucl. Data Tables* **71** 69
[13] Deb N C and Msezane A Z 2001 *Phys. Scr.* **64** 212
[14] Gupta G P and Msezane A Z 2008 *Phys. Scr.* **77** 035303
[15] Farrag A, Luc-Koenig E and Sinzelle J 1982 *At. Data Nucl. Data Tables* **27** 539
[16] Fawcett B C 1983 *At. Data Nucl. Data Tables* **28** 557
[17] Huang K-N 1986 *At. Data Nucl. Data Tables* **34** 1
[18] Mendoza C, Eissner W, Le Dourneuf M and Zeippen C J 1995 *J. Phys. B: At. Mol. Opt. Phys.* **28** 3485
[19] Safronova U I, Namba C, Albritton J R, Johnson W R, Safronova M S 2002 *Phys. Rev.* A **65** 022507
[20] Safronova U I, Sataka M, Albritton J R, Johnson W R and Safronova M S 2003 *At. Data Nucl. Data Tables* **84** 1
[21] FischerC F, TachievG and IrimiaA 2006 *At. Data Nucl. Data Tables* **92** 607
[22] Wei H L, Zhang H, Ma C W, Zhang J Y and Cheng X L 2008 Phys. Scr. 77 035301
[23] Träbert E, Hutton R and Martinson I 1987 *Z. Phys.* B **5** 125
[24] Träbert E, Heckmann P H, Hutton R and Martinson I 1988 *J. Opt. Soc. Am.* B **5** 2173
[25] Sugar J, Kaufman V and Rowan W L 1988 *J. Opt. Soc. Am.* B **5** 2183
[26] Redfors A and Litén U 1989 *J. Opt. Soc. Am.* B **6** 1447
[27] Ekberg J O, Redfors A, Brown C M, Feldman U and Seely JF 1991 *Phys. Scr.* **44** 539
[28] Raineri M, Bredice F, Gallardo M, Almandos J G R 1992 *Phys. Scr.* **45** 584
[29] Shirai T, Nakagaki T, Sugar J and Wiese W L 1992 *J. Phys. Chem. Ref. Data* **21** 273
[30] Shirai T, Nakai Y, Nakagaki T, Sugar J and Wiese W L 1993 *J. Phys. Chem. Ref. Data* **22** 1279
[31] Shirai T, Nakagaki T, Okazaki K, Sugar J and Wiese W L 1994 *J. Phys. Chem. Ref. Data* **23** 179
[32] Shirai T, Funatake Y, Mori K, Sugar J, Wiese W L and Nakai Y 1990 *J. Phys. Chem. Ref. Data* **19** 127
[33] Shirai T, Mengoni A, Nakai Y, Sugar J, Wiese W L, Mori K and Sakai H 1992 *J. Phys. Chem. Ref. Data* **21** 23
[34] Shirai T, K Mori, Sugar J, Wiese W L, Nakai Y, Ozawa K 1987 *At. Data Nucl. Data Tables* **37** 235

[35] Shirai T, Nakagaki T, Nakai Y, Sugar J, Ishii K and Mori K 1991 *J. Phys. Chem. Ref. Data* **20** 1
[36] Shirai T, Reader J, Kramida A E and Sugar J 2007 *J. Phys. Chem. Ref. Data* **36** 509
[37] Shirai T, Nakai Y, Ozawa K, Ishii K, Sugar J and Mori K 1987 J*J. Phys. Chem. Ref. Data* **16** 327
[38] Shirai T, K Okazaki and Sugar J 1995 *J. Phys. Chem. Ref. Data* **24** 1577
[39] Shirai T, Sugar J, Musgrove A and Wiese W L 2000 American Chemical Society and American Institute of Physics for
[40] Träbert E, Suleiman J, Cheng S, Berry H G, Dunford R W, Kanter E W, Kurtz C, Livingston A E, Kukla K W, Serpa F G and Curtis L J 1993 *Phys. Rev.* A **47** 3805
[41] Hutton R 1997 *Phys. Scr.* T **73** 25
[42] Bengtsson P, Ando K, Kambara T, Awaya Y and Hutton R 1997 *Phys. Scr.* T **73** 81
[43] Träbert E, Staude U, Bosselmann P, Schartner K H, Mokler P H and Tordoir X 1998 *Eur. Phys. J.* D **2** 117
[44] Vilkas M J, Ishikawa Y and Träbert E 2006 *Eur. Phys. J.* D **41** 77
[45] Redfors A and Litzén U 1988 *Phys. Lett.* A **127** 88
[46] Jupén and Curtis L J 1996 *Phys. Scr.* **53** 312
[47] Träbert E, Wagner C, Heckmann P H, Möller G and Brage T 1993 *Phys. Scr.* **48** 593
[48] Churilov S S and Levashov V E 1993 *Phys. Scr.* **48** 425
[49] Vilkas M J and Ishikawa Y 2005 *Phys. Rev.* A **72** 032512
[50] Vilkas M J and Ishikawa Y 2003 *Phys. Rev.* A **68** 012503
[51] Ralchenko Yu, Jou F-C, Kelleher D E, Kramida A E, Musgrove A, Reader J, Wiese W L and Olsen K 2005 *NIST Atomic Spectra Database (version 3.0.2)*, Online available at `http://physics.nist.gov/asd3` , National Institute of Standards and Technology, Gaithersburg, MD, USA
[52] Engström L, Kirm M, Bengtsson P, Maniak S T, Curtis L J, Träbert E, Doerfert J and Granzow J 1995 *Phys. Scr.* **52** 516
[53] Cowan R D, *The theory of atomic structure and spectra*, University of California Press, Berkeley, 1981.
[54] Vilkas M J, Ishikawa Y and Träbert E 2006 *J. Phys. B: At. Mol. Opt. Phys.* **39** 2195
[55] Vilkas M J and Ishikawa Y 2002 *Phys. Scr.* **65** 219
[56] Vilkas M J and Ishikawa Y 2003 *J. Phys. B: At. Mol. Opt. Phys.* **36** 4641
[57] Vilkas M J and Ishikawa Y 2004 *J. Phys. B: At. Mol. Opt. Phys.* **37** 1803
[58] Vilkas M J and Ishikawa Y 2004 *J. Phys. B: At. Mol. Opt. Phys.* **37** 4763
[59] Vilkas M J and Ishikawa Y 2004 *Phys. Rev.* A **69** 062503
[60] Vilkas M J, Ishikawa Y and Träbert E 2005 *Phys. Scr.* **72** 181
[61] Vilkas M J, Ishikawa Y and Koc K 1998 *Phys. Rev.* E **58** 5096
[62] Ishikawa Y, Koc K and Schwarz W H E 1997 *Chem. Phys.* **225** 239
[63] Ishikawa Y, Quiney H M, and Malli G L 1991 *Phys. Rev.* A **43** 3270
[64] Indelicato P, Gorceix O and Desclaux J P 1987 *J. Phys. B: At. Mol. Opt. Phys.* **20** 651
[65] Träbert E 2004 *Astron. Astrophys.* **415** L39
[66] Beiersdorfer P, Träbert E and Pinnington E H 2003 *Astrophys. J.* **587** 836
[67] Lapierre A, Crespo López-Urrutia J R, Braun J, Brenner G, Bruhns H, Fischer D, González-Martínez A J, Mironov V, Osborne C J, Sikler G, Soria Orts R, Tawara H, Ullrich J, Shabaev V M, Tupitsyn I I and Volotka A 2006 *Phys. Rev.* A **73** 052507
[68] Brenner G, Crespo López-Urrutia J R, Harman Z, Mokler P H and Ullrich J 2007 *Phys. Rev.* A **75** 032504
[69] Calamai A G, Smith P L and Bergeson S D 1993 *Astrophys. J.* **415** L59
[70] Träbert E, Hoffmann J, Krantz C, Wolf A, Ishikawa Y and Santana J A 2008 *J. Phys. B: At. Mol. Opt. Phys.* **42** (in print)
[71] Träbert E, Gwinner G, Wolf A, Knystautas E J, Garnir H-P and Tordoir X 2002 *J. Phys. B: At. Mol. Opt. Phys.* **35** 671

Table 1. Comparison of second-order MR-MP calculated energies and NIST experimental values in K^{6+}. The levels are identified in table 8.

Index	Parity	J	MR-MP	NIST	Deviation (percent)
1	o	1/2	0	0	0
2	o	3/2	3135	3134	0.032
3	e	1/2	114845	114650	0.170
4	e	3/2	115988	115786	0.174
5	e	5/2	117726	117523	0.173
6	e	3/2	151859	151883.9	0.016
7	e	5/2	152028	152051.7	0.016
8	e	1/2	193146	193084.5	0.032
9	e	1/2	206554	206502.9	0.025
10	e	3/2	208484	208432.5	0.025
11	e	3/2	250943	250663	0.112
12	e	5/2	251070	250781	0.115
13	o	3/2	297753		
14	o	5/2	298062		
15	o	3/2	307968	307777	0.062
16	o	3/2	334167		
17	o	5/2	334811		
18	o	1/2	335349		
19	o	3/2	335380		
20	o	7/2	335734		
21	o	9/2	336959		
22	o	5/2	362840	362492	0.096
23	o	3/2	363682	363321	0.099
24	o	1/2	364381		
25	o	1/2	366070	365688	0.104
26	o	3/2	366476	366101	0.102
27	o	5/2	366811	366409	0.110
28	o	7/2	366978	366556	0.115
29	o	5/2	376542		
30	o	3/2	376571		
31	o	5/2	394592		
32	o	7/2	397091		
33	o	3/2	431251		
34	o	1/2	432181		
35	o	7/2	432891		
36	o	5/2	433529		
37	o	1/2	447334		
38	o	3/2	447478		
39	o	3/2	451899		
40	o	5/2	452353		

Table 2. Comparison of second-order MR-MP calculated energies and NIST experimental values in Ca^{7+}. The levels are identified in table 8.

Index	Parity	J	MR-MP	NIST	Deviation (percent)
1	o	1/2	0	0	0
2	o	3/2	4307	4308.3	0.030
3	e	1/2	129796	129100	0.539
4	e	3/2	131382	130678	0.539
5	e	5/2	133745	133042	0.528
6	e	3/2	171537	171572.2	0.021
7	e	5/2	171789	171830.7	0.024
8	e	1/2	216548	216584.9	0.017
9	e	1/2	231037	231016.3	0.009
10	e	3/2	233614	233592.8	0.009
11	e	3/2	282539	282356	0.065
12	e	5/2	282765	282577	0.067
13	o	3/2	335800		
14	o	5/2	336255		
15	o	3/2	345942	345274	0.193
16	o	1/2	376944		
17	o	3/2	377077		
18	o	3/2	377423		
19	o	5/2	378315		
20	o	7/2	379596		
21	o	9/2	381304		
22	o	5/2	409030	408227	0.197
23	o	3/2	410107	409291	0.199
24	o	1/2	411080	411816	0.179
25	o	1/2	412581		
26	o	3/2	413178	412388	0.192
27	o	5/2	413592	412772	0.199
28	o	7/2	413742	412881	0.209
29	o	5/2	423788		
30	o	3/2	423802		
31	o	5/2	444185		
32	o	7/2	447611		
33	o	3/2	484543		
34	o	1/2	485933		
35	o	7/2	487088		
36	o	5/2	487944		
37	o	1/2	502416		
38	o	3/2	502700		
39	o	3/2	506781		
40	o	5/2	507392		

Table 3. Comparison of second-order MR-MP calculated energies and NIST experimental values in Sc^{7+}. The levels are identified in table 8.

Index	Parity	J	MR-MP	NIST	Deviation (percent)
1	o	1/2	0	0	0
2	o	3/2	5764	5761.1	0.050
3	e	1/2	144970	143500	1.024
4	e	3/2	147118	145622	1.027
5	e	5/2	150249	148779	0.988
6	e	3/2	191573	191609.3	0.019
7	e	5/2	191946	191987.1	0.021
8	e	1/2	240433	240361.4	0.030
9	e	1/2	255853	255829.4	0.009
10	e	3/2	259180	259153.7	0.010
11	e	3/2	313992	313860	0.042
12	e	5/2	314357	314214	0.046
13	o	3/2	374303		
14	o	5/2	374966		
15	o	3/2	384478	383047	0.374
16	o	1/2	419256		
17	o	3/2	419568		
18	o	3/2	420737		
19	o	5/2	421944		
20	o	7/2	423676		
21	o	9/2	426000		
22	o	5/2	455201		
23	o	3/2	456505		
24	o	1/2	457719		
25	o	1/2	459344		
26	o	3/2	460090		
27	o	5/2	460545		
28	o	7/2	460636		
29	o	3/2	471276		
30	o	5/2	471294		
31	o	5/2	493692		
32	o	7/2	498272		
33	o	3/2	537741		
34	o	1/2	539716		
35	o	7/2	541243		
36	o	5/2	542357		
37	o	1/2	557502		
38	o	3/2	558022		
39	o	3/2	561660		
40	o	5/2	562455		

Table 4. Comparison of second-order MR-MP calculated energies and NIST experimental values in Ti^{9+}. The levels are identified in table 8.

Index	Parity	J	MR-MP	NIST	Deviation (percent)
1	o	1/2	0	0	0
2	o	3/2	7543	7544	0.013
3	e	1/2	160412	160409	0.002
4	e	3/2	163265	163257	0.005
5	e	5/2	167320	167309	0.007
6	e	3/2	212025	212053	0.013
7	e	5/2	212574	212608	0.016
8	e	1/2	264594	264456	0.052
9	e	1/2	281072	281051	0.007
10	e	3/2	285238	285220	0.006
11	e	3/2	345411	345315	0.028
12	e	5/2	345963	345859	0.030
13	o	3/2	413358	413397	0.009
14	o	5/2	414317	414365	0.012
15	o	3/2	423669	423713	0.010
16	o	1/2	462184	462142	0.009
17	o	3/2	462767	462709	0.013
18	o	3/2	464235		
19	o	5/2	465834	465910	0.016
20	o	7/2	468125	468204	0.017
21	o	9/2	471220	471285	0.014
22	o	5/2	501506	501474	0.006
23	o	3/2	503018	502940	0.016
24	o	1/2	504332	504163	0.034
25	o	1/2	506701	506849	0.029
26	o	3/2	507443	507492	0.010
27	o	7/2	507871	507815	0.011
28	o	5/2	507884	507859	0.005
29	o	3/2	519127	519034	0.018
30	o	5/2	519198	519113	0.016
31	o	5/2	543235	543166	0.013
32	o	7/2	549227	549148	0.014
33	o	3/2	590926	590439	0.082
34	o	1/2	593650	593151	0.084
35	o	7/2	595519	595023	0.083
36	o	5/2	596931	596470	0.077
37	o	1/2	612842	612628	0.035
38	o	3/2	613542	613252	0.047
39	o	3/2	616710	616264	0.072
40	o	5/2	617699	617188	0.083

Table 5. Comparison of second-order MR-MP calculated energies and NIST experimental values in V^{10+}. The levels are identified in table 8.

Index	Parity	J	MR-MP	NIST	Deviation (percent)
1	o	1/2	0	0	0
2	o	3/2	9694	9696	0.021
3	e	1/2	176107	176117	0.006
4	e	3/2	179836	179839	0.002
5	e	5/2	184987	184992	0.003
6	e	3/2	232943	232972	0.012
7	e	5/2	233738	233778	0.017
8	e	1/2	288991	288914	0.027
9	e	1/2	306803	306801	0.001
10	e	3/2	311892	311890	0.001
11	e	3/2	376922	376897	0.007
12	e	5/2	377722	377650	0.019
13	o	3/2	453014	453057	0.009
14	o	5/2	454387	454448	0.013
15	o	3/2	463584	463653	0.015
16	o	1/2	505716	505765	0.010
17	o	3/2	506716	506695	0.004
18	o	3/2	507982		
19	o	5/2	510059	510204	0.028
20	o	7/2	513033	513127	0.018
21	o	9/2	517082	517171	0.017
22	o	5/2	548038	548037	0.000
23	o	3/2	549745	549713	0.006
24	o	1/2	551073	550994	0.014
25	o	1/2	554732	554864	0.024
26	o	3/2	555373	555472	0.018
27	o	7/2	555589	555583	0.001
28	o	5/2	555748	555759	0.002
29	o	3/2	567493	567465	0.005
30	o	5/2	567645	567610	0.006
31	o	5/2	592986	592959	0.005
32	o	7/2	600681	600643	0.006
33	o	3/2	644322	643917	0.063
34	o	1/2	647995	647577	0.065
35	o	7/2	650132	649771	0.056
36	o	5/2	651881	651550	0.051
37	o	1/2	668547	668411	0.020
38	o	3/2	669536	669304	0.035
39	o	3/2	672173	671902	0.040
40	o	5/2	673362	672939	0.063

Table 6. Comparison of second-order MR-MP calculated energies and NIST experimental values in Cr^{11+}. The levels are identified in table 8.

Index	Parity	J	MR-MP	NIST	Deviation (percent)
1	o	1/2	0	0	0
2	o	3/2	12262	12261	0.008
3	e	1/2	192096	192120	0.012
4	e	3/2	196900	196911	0.006
5	e	5/2	203332	203349	0.008
6	e	3/2	254402	254428	0.010
7	e	5/2	255537	255566	0.011
8	e	1/2	313809	313745	0.020
9	e	1/2	333197	333196	0.000
10	e	3/2	339257	339251	0.002
11	e	3/2	408659	408640	0.005
12	e	5/2	409776	409741	0.009
13	o	3/2	493361	493437	0.015
14	o	5/2	495309	495368	0.012
15	o	3/2	504345	504431	0.017
16	o	1/2	550161	550208	0.009
17	o	3/2	551751	551641	0.020
18	o	3/2	552098		
19	o	5/2	554738	554899	0.029
20	o	7/2	558535	558684	0.027
21	o	9/2	563750	563915	0.029
22	o	5/2	594933	594946	0.002
23	o	3/2	596839	596837	0.000
24	o	1/2	598195	598172	0.004
25	o	1/2	603492	603600	0.018
26	o	7/2	603967	603995	0.005
27	o	3/2	604035	604158	0.020
28	o	5/2	604304	604331	0.004
29	o	3/2	616538	616498	0.006
30	o	5/2	616805	616790	0.002
31	o	5/2	643104	643089	0.002
32	o	7/2	652825	652796	0.004
33	o	3/2	698116	697756	0.052
34	o	1/2	702965		
35	o	7/2	705269	704993	0.039
36	o	5/2	707396	707142	0.036
37	o	1/2	724795	724656	0.019
38	o	3/2	726053	725710	0.047
39	o	3/2	728341	728200	0.019
40	o	5/2	729650	729281	0.051

Table 7. Comparison of second-order MR-MP calculated energies and NIST experimental values in Mn^{12+}. The levels are identified in table 8.

Index	Parity	J	MR-MP	NIST	Deviation (percent)
1	o	1/2	0	0	0
2	o	3/2	15296	15295	0.007
3	e	1/2	208409	208451	0.020
4	e	3/2	214524	214546	0.010
5	e	5/2	222434	222463	0.013
6	e	3/2	276474	276497	0.008
7	e	5/2	278072	278099	0.010
8	e	1/2	339052	339001	0.015
9	e	1/2	360388	360387	0.000
10	e	3/2	367435	367425	0.003
11	e	3/2	440719	440725	0.001
12	e	5/2	442231	442220	0.002
13	o	3/2	534469	534492	0.004
14	o	5/2	537209	537263	0.010
15	o	3/2	546074	546178	0.019
16	o	1/2	595629	595637	0.001
17	o	3/2	596675		
18	o	3/2	598030	597797	0.039
19	o	5/2	599975		
20	o	7/2	604753		
21	o	9/2	611382	611495	0.018
22	o	5/2	642308	642337	0.005
23	o	3/2	644434	644449	0.002
24	o	1/2	645847	645856	0.001
25	o	1/2	653099	653189	0.014
26	o	7/2	653163	653217	0.008
27	o	3/2	653564	653697	0.020
28	o	5/2	653698	653739	0.006
29	o	3/2	666406	666369	0.006
30	o	5/2	666826	666826	0.000
31	o	5/2	693721	693715	0.001
32	o	7/2	705826	705799	0.004
33	o	3/2	752439	752115	0.043
34	o	1/2	758731		
35	o	7/2	761090	760881	0.027
36	o	5/2	763631	763441	0.025
37	o	1/2	781730	781703	0.003
38	o	3/2	783168	782845	0.041
39	o	3/2	785474	785391	0.011
40	o	5/2	786733	786405	0.042

Table 8. Comparison of second-order MR-MP calculated energies and NIST experimental values in Fe^{13+}.

Configuration	Index	Level	MR-MP	NIST	Deviation (percent)
$3s^2 3p$	1	$^2P^o_{1/2}$	0	0	0
	2	$^2P^o_{3/2}$	18852	18852.5	0.003
$3s3p^2$	3	$^4P_{1/2}$	225090	225114	0.011
	4	$^4P_{3/2}$	232794	232789	0.002
	5	$^4P_{5/2}$	242386	242387	0.000
	6	$^2D_{3/2}$	299231	299242	0.004
	7	$^2D_{5/2}$	301452	301469	0.006
	8	$^2S_{1/2}$	364717	364693	0.007
	9	$^2P_{1/2}$	388502	388510	0.002
	10	$^2P_{3/2}$	396516	396512	0.001
$3s^2 3d$	11	$^2D_{3/2}$	473188	473223	0.007
	12	$^2D_{5/2}$	475185	475202	0.001
$3p^3$	13	$^2D^o_{3/2}$	576407	576388	0.004
	14	$^2D^o_{5/2}$	580226	580233	0.001
	15	$^4S^o_{3/2}$	588916	589002	0.015
	16	$^2P^o_{1/2}$	642236	642310	0.012
	17	$^2P^o_{3/2}$	645732	645409	0.050
$3s3p[^3P]3d$	18	$^4F^o_{3/2}$	641822		
	19	$^4F^o_{5/2}$	645891	645988	0.015
	20	$^4F^o_{7/2}$	651824	651946	0.019
	21	$^4F^o_{9/2}$	660153	660263	0.017
	22	$^4P^o_{5/2}$	690300	690304	0.001
	23	$^4D^o_{3/2}$	692673	692662	0.002
	24	$^4D^o_{1/2}$	694166	694166	0.000
	25	$^4D^o_{7/2}$	703359	703393	0.005
	26	$^4P^o_{1/2}$	703723	703750	0.004
	27	$^4D^o_{5/2}$	704095	704114	0.003
	28	$^4P^o_{3/2}$	704123	704209	0.012
	29	$^4D^o_{3/2}$	717245	717195	0.007
	30	$^4D^o_{5/2}$	717863	717861	0.000
	31	$^4F^o_{5/2}$	744955	744965	0.001
	32	$^4P^o_{7/2}$	759833	759814	0.003
	33	$^4P^o_{3/2}$	807380	807113	0.033
	34	$^4P^o_{1/2}$	815419	815123[a]	0.036
$3s3p[^1P]3d$	35	$^4F^o_{7/2}$	817734	817593	0.017
	36	$^4F^o_{5/2}$	820724	820601	0.015
	37	$^4P^o_{1/2}$	839475	839492	0.002
	38	$^4D^o_{3/2}$	841040	840775	0.032
	39	$^4P^o_{3/2}$	843700	843656	0.005
	40	$^4D^o_{5/2}$	844757	844477	0.033

Table 9. Comparison of second-order MR-MP calculated energies and NIST experimental values in Co^{14+}. The levels are identified in table 8.

Index	Parity	J	MR-MP	NIST	Deviation (percent)
1	o	1/2	0	0	0
2	o	3/2	22987	22979	0.035
3	e	1/2	242094	242124	0.012
4	e	3/2	251709	251699	0.004
5	e	5/2	263194	263189	0.002
6	e	3/2	322723	322725	0.001
7	e	5/2	325772	325790	0.006
8	e	1/2	390874	390855	0.005
9	e	1/2	417713	417717	0.001
10	e	3/2	426634	426629	0.001
11	e	3/2	506176	506230	0.011
12	e	5/2	508756	508793	0.007
13	o	3/2	619153	619050	0.017
14	o	5/2	624416	624445	0.005
15	o	3/2	632936	633036	0.016
16	o	3/2	687552		
17	o	1/2	690102	690171	0.010
18	o	5/2	692512	692464	0.007
19	o	3/2	695034	694620	0.060
20	o	7/2	699794	699778	0.002
21	o	9/2	710151	710230	0.011
22	o	5/2	738948	738955	0.001
23	o	3/2	741601	741602	0.000
24	o	1/2	743187	743224	0.005
25	o	7/2	754639	754674	0.005
26	o	1/2	755443		
27	o	5/2	755568	755594	0.003
28	o	3/2	755783		
29	o	3/2	769173	769138	0.005
30	o	5/2	770032	770046	0.002
31	o	5/2	796959	796989	0.004
32	o	7/2	815026	815014	0.001
33	o	3/2	863127	862878	0.029
34	o	1/2	873267		
35	o	7/2	875384	875288	0.011
36	o	5/2	878849	878778	0.008
37	o	1/2	898217	898240	0.003
38	o	3/2	899955	899693	0.029
39	o	3/2	903160	903152	0.001
40	o	5/2	903931	903677	0.028

Table 10. Comparison of second-order MR-MP calculated energies and NIST experimental values in Ni^{15+}. The levels are identified in table 8.

Index	Parity	J	MR-MP	NIST	Deviation (percent)
1	o	1/2	0	0	0
2	o	3/2	27759	27760.4	0.005
3	e	1/2	259466	259489	0.009
4	e	3/2	271367	271341	0.010
5	e	5/2	284954	284949	0.002
6	e	3/2	347030	347032	0.001
7	e	5/2	351166	351185	0.005
8	e	1/2	417542	417523	0.005
9	e	1/2	448160	448169	0.002
10	e	3/2	457900	457912	0.003
11	e	3/2	539769	539839	0.013
12	e	5/2	543041	543107	0.012
13	o	3/2	662774	662678	0.014
14	o	5/2	669939	669946	0.001
15	o	3/2	678316	678418	0.015
16	o	3/2	733983		
17	o	1/2	739369	739500	0.018
18	o	5/2	739964		
19	o	3/2	746137	746100	0.005
20	o	7/2	748806		
21	o	9/2	761568	761641	0.010
22	o	5/2	788390	788399	0.001
23	o	3/2	791357	791390	0.004
24	o	1/2	793043	793115	0.009
25	o	7/2	807192	807214	0.003
26	o	5/2	808291	808316	0.003
27	o	1/2	808438		
28	o	3/2	808721		
29	o	3/2	822351	822364	0.002
30	o	5/2	823484	823538	0.007
31	o	5/2	849869	849946	0.009
32	o	7/2	871561	871583	0.003
33	o	3/2	919765	919543	0.024
34	o	1/2	932400		
35	o	7/2	934186	934137	0.005
36	o	5/2	938146	938122	0.003
37	o	1/2	958094	958134	0.004
38	o	3/2	960119		
39	o	3/2	963960	963961	0.000
40	o	5/2	964409		

Table 11. Comparison of second-order MR-MP calculated energies and NIST experimental values in Cu^{16+}. The levels are identified in table 8.

Index	Parity	J	MR-MP	NIST	Deviation (percent)
1	o	1/2	0	0	0
2	o	3/2	33235	33239	0.012
3	e	1/2	277216	277231	0.005
4	e	3/2	291837	291810	0.009
5	e	5/2	307733	307708	0.008
6	e	3/2	372227	372236	0.002
7	e	5/2	377770	377783	0.003
8	e	1/2	444775	444759	0.004
9	e	1/2	479992	480016	0.005
10	e	3/2	490438	490467	0.006
11	e	3/2	574060	574180	0.021
12	e	5/2	578141	578243	0.018
13	o	3/2	707310		
14	o	5/2	716925		
15	o	3/2	725208	725320	0.015
16	o	3/2	781201		
17	o	5/2	788341		
18	o	1/2	790181		
19	o	7/2	798971		
20	o	3/2	799245		
21	o	9/2	814569		
22	o	5/2	838734		
23	o	3/2	842050		
24	o	1/2	843832		
25	o	7/2	861178	861003	0.020
26	o	5/2	862412	856728	0.663
27	o	1/2	862861		
28	o	3/2	863087		
29	o	3/2	876925		
30	o	5/2	878344	876785	0.178
31	o	5/2	903850	909161	0.584
32	o	7/2	929605	931186	0.170
33	o	3/2	977417		
34	o	1/2	992982		
35	o	7/2	994301		
36	o	5/2	998764		
37	o	1/2	1019261		
38	o	3/2	1021739		
39	o	3/2	1026248		
40	o	5/2	1026365		

Table 12. Comparison of second-order MR-MP calculated energies and NIST experimental values in Zn^{17+}. The levels are identified in table 8.

Index	Parity	J	MR-MP	NIST	Deviation (percent)
1	o	1/2	0	0	0
2	o	3/2	39479	39483	0.010
3	e	1/2	295343	295200	0.048
4	e	3/2	313181	312993	0.060
5	e	5/2	331582	331359	0.067
6	e	3/2	398381	398390	0.002
7	e	5/2	405728	405760	0.008
8	e	1/2	472635	472601	0.007
9	e	1/2	513359	513373	0.003
10	e	3/2	524378	524382	0.001
11	e	3/2	609150	609252	0.017
12	e	5/2	614166	614272	0.017
13	o	3/2	752796		
14	o	5/2	765496		
15	o	3/2	773750	773682	0.009
16	o	3/2	829286		
17	o	5/2	837734		
18	o	1/2	842676		
19	o	7/2	850395		
20	o	3/2	854547		
21	o	9/2	869318		
22	o	5/2	890082		
23	o	3/2	893782		
24	o	1/2	895643		
25	o	7/2	916758		
26	o	5/2	918075		
27	o	1/2	918860		
28	o	3/2	919028		
29	o	3/2	933041		
30	o	5/2	934708		
31	o	5/2	959094		
32	o	7/2	989327		
33	o	3/2	1036210		
34	o	1/2	1055173		
35	o	7/2	1055896		
36	o	5/2	1060860		
37	o	1/2	1081888		
38	o	3/2	1085020		
39	o	5/2	1089979		
40	o	3/2	1090194		

Table 13. Comparison of second-order MR-MP calculated energies and NIST experimental values in Ga^{18+}. The levels are identified in table 8.

Index	Parity	J	MR-MP	NIST	Deviation (percent)
1	o	1/2	0	0	0
2	o	3/2	46564	46584	0.043
3	e	1/2	313855		
4	e	3/2	335482		
5	e	5/2	356566		
6	e	3/2	425572	425568	0.001
7	e	5/2	435204	435260	0.013
8	e	1/2	501201	501163	0.008
9	e	1/2	548416	548398	0.003
10	e	3/2	559855	559837	0.003
11	e	3/2	645141	645235	0.015
12	e	5/2	651220	651354	0.021
13	o	3/2	799298		
14	o	5/2	815793		
15	o	3/2	824097		
16	o	3/2	878333		
17	o	5/2	888243		
18	o	1/2	897017		
19	o	7/2	903190		
20	o	3/2	912241		
21	o	9/2	925995		
22	o	5/2	942546		
23	o	3/2	946678		
24	o	1/2	948576		
25	o	7/2	974103		
26	o	5/2	975440		
27	o	1/2	976601		
28	o	3/2	976708		
29	o	3/2	990850		
30	o	5/2	992636		
31	o	5/2	1015851		
32	o	7/2	1050903		
33	o	3/2	1096284		
34	o	1/2	1119143		
35	o	7/2	1119148		
36	o	5/2	1124592		
37	o	1/2	1146149		
38	o	3/2	1150163		
39	o	5/2	1155438		
40	o	3/2	1155981		

Table 14. Comparison of second-order MR-MP calculated energies and NIST experimental values in Ge^{19+}. The levels are identified in table 8.

Index	Parity	J	MR-MP	NIST	Deviation (percent)
1	o	1/2	0	0	0
2	o	3/2	54562	54564	0.004
3	e	1/2	332749		
4	e	3/2	358815		
5	e	5/2	382743		
6	e	3/2	453877	453869	0.002
7	e	5/2	466367	466407	0.009
8	e	1/2	530558	530521	0.007
9	e	1/2	585318	585257	0.010
10	e	3/2	597008	597020	0.002
11	e	3/2	682141	682246	0.015
12	e	5/2	689414	689533	0.017
13	o	3/2	846885		
14	o	5/2	867950		
15	o	3/2	876391	875850	0.062
16	o	3/2	928436		
17	o	5/2	939968		
18	o	1/2	953363		
19	o	7/2	957466		
20	o	3/2	972492	1000790	
21	o	9/2	984782	1002640	
22	o	5/2	996239	996200	0.004
23	o	3/2	1000881		
24	o	1/2	1002722		
25	o	7/2	1033390	1033390	0.000
26	o	5/2	1034665		
27	o	1/2	1036246	1035630	0.059
28	o	3/2	1036292		
29	o	3/2	1050501	1050590	0.008
30	o	5/2	1052112		
31	o	5/2	1074450		
32	o	7/2	1114514	1114490	0.002
33	o	3/2	1157787	1157630	0.014
34	o	7/2	1184236	1184750	0.043
35	o	1/2	1185058	1184190	0.073
36	o	5/2	1190124	1190040	0.007
37	o	1/2	1212228	1211960	0.022
38	o	3/2	1217365	1217450	0.007
39	o	5/2	1222930	1222780	0.012
40	o	3/2	1223805	1223700	0.009

Table 15. Calculated E1/M1/E2/M2 transition probabilities A and lifetimes τ of $3s23p^2P^o_{3/2}$, $3s3p^2\ ^4P_J$, and $3s3p3d\ ^4F^o_{9/2}$ levels in aluminium-like Fe^{13+}. a(b) means a$\times 10^b$.

Upper(j) → Lower (i)	ΔE (cm^{-1})	A_{ji}(s^{-1})	τ (μs)
Fe^{+13}			
$^2P^o_{3/2} \rightarrow\ ^2P^o_{1/2}$	18852	M1: 6.016(+1)	
		E2: 1.466(-2)^B	16620
		1.484(-2)^C	
$^4F^o_{9/2} \rightarrow\ ^4F^o_{7/2}$	8329	M1: 1.541(+1)	
		E2: 1.628(-4)^B	
		1.724(-4)^C	
$\rightarrow\ ^4F^o_{5/2}$	14262	E2: 2.096(-4)^B	
		2.228(-4)^C	
$\rightarrow\ ^2D^o_{5/2}$	79927	E2: 2.691(-3)^B	
		2.875(-3)^C	
$\rightarrow\ ^2D_{5/2}$	184968	M2: 2.423(-1)	
$\rightarrow\ ^2D_{5/2}$	358701	M2: 3.375(+1)	
$\rightarrow\ ^4P_{5/2}$	417767	M2: 3.361(+0)	18950
$^4P_{5/2} \rightarrow\ ^4P_{3/2}$	9592	M1: 1.411(+1)	
		E2: 4.976(-4)^B	
		5.097(-4)^C	
$\rightarrow\ ^4P_{1/2}$	17296	E2: 3.274(-3)^B	
		7.160(-3)^C	
$\rightarrow\ ^2P^o_{3/2}$	223534	E1: 2.256(+7)^B	
		2.064(+7)^C	
		M2: 1.685(+0)	
$\rightarrow\ ^2P^o_{1/2}$	242386	M2: 1.423(+0)	0.04433
$^4P_{3/2} \rightarrow\ ^4P_{1/2}$	7704	M1: 1.014(+1)	
		E2: 1.003(-5)^B	
		2.099(-5)^C	
$\rightarrow\ ^2P^o_{3/2}$	213942	E1: 5.458(+6)^B	
		4.851(+6)^C	
		M2: 6.838(-2)	
$\rightarrow\ ^2P^o_{1/2}$	232794	E1: 4.833(+5)^B	
		4.640(+5)^C	
		M2: 2.193(+0)	0.1683
$^4P_{1/2} \rightarrow\ ^4P^o_{3/2}$	206238	M2: 2.892(-1)	
		E1: 8.693(+6)^B	
		7.885(+6)^C	
$\rightarrow\ ^2P^o_{1/2}$	225090	E1: 2.230(+7)^B	0.0323

^{B} in Babushkin gauge; ^{C} in Coulomb gauge

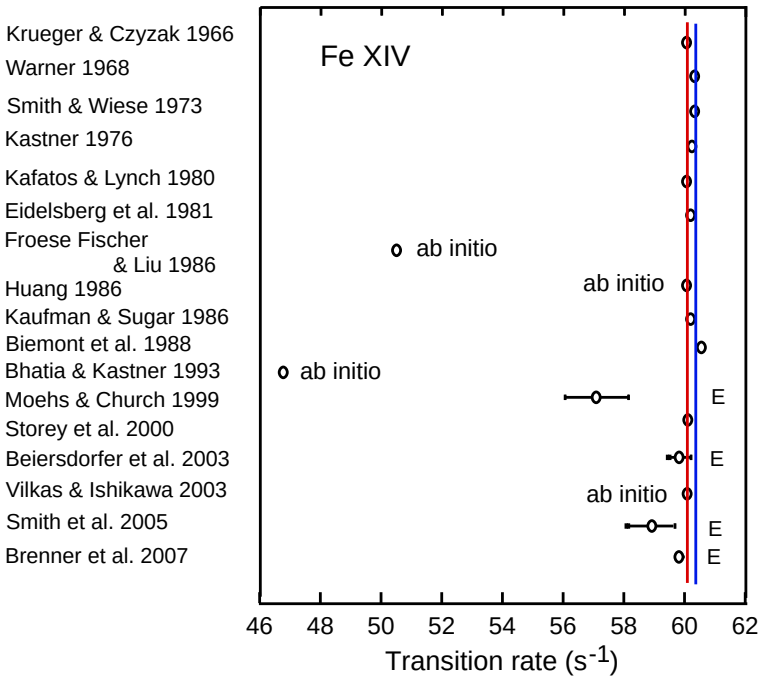

Figure 1. (Colour online) Historic timeline of the calculated and measured (E) M1 transition rate in the ground state of Fe XIV. The vertical red (left) line indicates the expected value based on the experimental term difference and a line strength $S = 4/3$; the vertical blue (right) line represents the same after the application of the QED correction to the M1 transition operator.

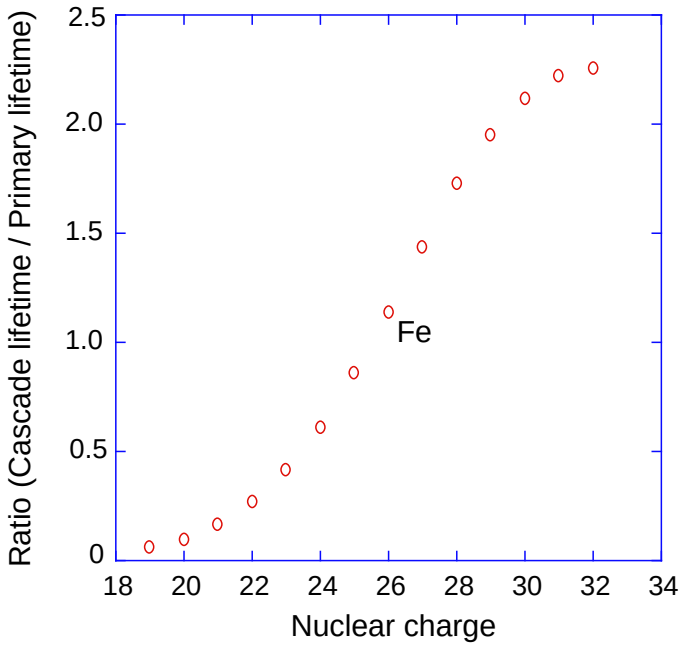

Figure 2. Ratio of lifetimes of the $3s3p3d\ {}^4\mathrm{F}^{\mathrm{o}}_{9/2}$ (cascade) and the $3s^23p\ {}^2\mathrm{P}^{\mathrm{o}}_{3/2}$ (primary decay) levels.

Table 16. Lifetime of the five long-lived levels among the lowest 40 levels of Al-like ions from K^{6+} to Ge^{19+}: $3s^23p^2\,{}^2\mathrm{P}^o_{3/2}$, $3s3p^2\,{}^4\mathrm{P}_{5/2,3/2,1/2}$, and $3s3p3d\,{}^4\mathrm{F}^o_{9/2}$.

Ion	$^2P^o_{3/2}$		$^4P_{5/2}$	$^4P_{3/2}$	$^4P_{1/2}$	$^4F^o_{9/2}$
	without	with				
	QED correction to the M1 operator					
	τ (ms)	τ (ns)	τ (ns)	τ (ns)	τ (ns)	τ (ms)
K^{6+}	3611	3595	2116	5719	1130	214.6
Ca^{7+}	1393	1387	1047	2941	574	142.2
Sc^{8+}	581.3	578.7	499	1517	250	97.62
Ti^{9+}	259.3	258.1	312	956	192	70.25
V^{10+}	122.2	121.7	182	586	117	50.83
Cr^{11+}	60.38	60.11	110	374	73.3	36.94
Mn^{12+}	31.11	30.97	69.0	247	47.5	26.67
Fe^{13+}	16.62	16.55	44.3	168	32.3	18.95
		16.74±0.12 [a]	39±5 [c]		29±3 [c]	
		16.726+0.02-0.01 [b]				
Co^{14+}	9.172	9.131	29.2	118	21.5	13.18
			26±1.5 [c]		18±1 [c]	
Ni^{15+}	5.207	5.184	19.7	84.3	14.9	8.933
		5.27±0.07 [d]	16±2 [c]		12±1.5 [c]	10±0.7 [d]
Cu^{16+}	3.034	3.020	13.5	61.6	10.6	5.910
			10.5±0.5 [c]		8.5±0.5 [c]	
Zn^{17+}	1.810	1.802	9.50	45.9	7.61	3.831
			7.5±1.0 [c]		8.3±0.6 [c]	
Ga^{18+}	1.104	1.099	6.81	34.8	5.56	2.449
Ge^{19+}	0.6859	0.6828	4.98	26.9	4.13	1.552

a [66]
b [68]
c [24]
d [70]